RSC Advances

This article can be cited before page numbers have been issued, to do this please use: F. Xu, J. Li, T. Zhu, S. Yu, C. Zuo, R. Yao and H. Qian, *RSC Adv.*, 2016, DOI: 10.1039/C6RA23440B.

View Article Online
DOI: 10.1039/C6RA23440B

A New Trick (Hydroxyl radical generation) of an Old Vitamin (B_2) for Near-infrared-triggered Photodynamic Therapy

Fang Xu*[, a], Jin Li[a], Ting-ting Zhu[a,b], Sheng-Song Yu[b], Chong Zuo[a], Ri-sheng Yao[a] and Hai-sheng Qian[a]

[a]Department of Pharmaceutical Engineering, Hefei University of Technology, Hefei, 230009, China; [b]Department of Chemistry, University of Science & Technology of China, Hefei, 230026, China.

Corresponding author:

Fang Xu, E-mail: Fangxu@hfut.edu.cn; Fax: +86 551 62901771

View Article Online
DOI: 10.1039/C6RA23440B

ABSTRACT:

Photosensitizer has been supposed to the key component in photodynamic therapy (PDT). Natural products and their intricate molecular frameworks are often used as starting points for drug discovery. Riboflavin (RF), also known as vitamin B_2, bearing a unique conjugate structure of isoalloxazine ring, is a potential photosensitizer for use in the PDT of cancers. In this study, we present a novel near-infrared (NIR) mediated nanocomposite for PDT, using this old vitamin as a PDT photosensitizer, integrated with the upconversion nanotechnology. Mesoporous-silica-coated $NaYF_4$:Yb/Tm nanoparticles were fabricated and used as drug carriers and photo-transducers. Chemical modification of RF was performed to obtain a photostable photosensitizer (2',3',4',5'-tetraacetylriboflavin, RTA). There is a good overlap between the fluorescence emission of $NaYF_4$:Yb/Tm nanoparticles and the UV-visible absorption of RTA. RTA molecules were incorporated into the mesoporous silica shell and the fluorescent emission from $NaYF_4$:Yb/Tm nanoparticles can be absorbed by RTA molecules under NIR irradiation. NIR-initiated reactive oxygen species generation was validated by electron paramagnetic resonance spectroscopy combined with spin trapping. The results from *in-vitro* cell test show good photodynamic efficacy of this nanocomposite. All ingredients involved in this process are nontoxic, environmentally benign, and easily-available. Thus, this nanocomposite might has great potential in PDT applications.

View Article Online
DOI: 10.1039/C6RA23440B

1. Introduction

Photodynamic therapy (PDT) has emerged as a promising and noninvasive treatment for various types of cancers, involving three key components: photosensitizer (PS, also called PDT drug), light source and tissue oxygen.[1-3] The combination of these three components leads to the generation of different reactive oxygen species (ROS), such as singlet oxygen ($^1O_2$) through a energy-transfer process (Type II mechanism), and superoxide anion radical ($O_2^{\bullet-}$) through a electron-transfer process (Type I mechanism).[4-6] Subsequently, ROS cause oxidative damage to biological substrates and ultimately result in cancer cell death.[7-9] This strategy has gained wide research interest as a powerful technique for cancer treatment, due to its built-in selectivity, low systemic toxicity, minimal invasiveness as well as the possibility of its use in combination with other anticancer therapies.

Among which, PS is the key agent in PDT application and is also the research focus in the PDT-related field.[10-16] In clinical practice, porphyrins and its derivatives, such as Photofrin (a mixture of hematoporphyrin monomers, dimers, and oligomers,) and Foscan (*m*-tetrahydroxyphenylchlorin), are the most commonly-used PDT PSs.[17] However, these compounds suffer from several drawbacks: (1) tedious synthesis and purification, (2) poor water solubility, and (3) slow clearance from the body leading to possible photosensitivity after PDT treatment.[18-24] Therefore, it is still imperative to develop efficient, highly photostable, and excellent water dispersible PSs. Features desired for ideal PDT drugs, including: (1) high photochemical reactivity, that is, it can effectively produce ROS under appropriate irradiation; (2) low dark toxicity; and (3) can be excited at a wavelength in the region where tissue penetration of irradiation is at a maximum.

View Article Online
DOI: 10.1039/C6RA23440B

Natural products and their intricate molecular frameworks are often used as starting points for drug discovery.[11, 25-27] Riboflavin (RF), also known as vitamin B_2, is an important vitamin and widely present both *in-vivo* and natural environments.[28-31] It contains a unique conjugate structure, called isoalloxazine ring, which has been reported to function as an excellent natural PS for the generation of ROS, such as $^1O_2$ and/or $O_2^{\bullet-}$.[32-34] In our previous studies, ROS generation, including highly reactive hydroxyl radical (•OH), has been validated during the photosensitization process of RF (**Fig. 1**). In which, RF play a dual role of photosensitizer and electron mediator.[35-37] All ingredients involved in this process are nontoxic, environmentally benign, and easily-available. Thus, this process might have broad medical implications and inspires us to probe the possibility of this vitamin working as a novel PDT drug.

However, this idea begs the following questions: (1) the limited penetration depth of the excitation wavelength of RF (<520 nm), which inflicts biological damage and cannot take advantage of the optical window of tissue (700-1100 nm),[32-39] and (2) the poor photostability of RF under UV or visible irradiations.[32-36] Nonlinear processes (involving more than one photon) have been investigated as a potential solution to address question (1). In this context, upconversion nanoparticles (UCNP), a photo-transducer capable of converting NIR light to UV or visible light, was employed as an excitation method for PDT treatment.[40-46] To further underline the feasibility of RF working as a PDT drug, 2',3',4',5'-tetraacetylriboflavin (RTA) was designed and synthetized from RF through a esterification process of its ribose chain with acetic anhydride.[34, 47-49]

In this study, RTA (a photostable derivative of RF) was used as a novel PDT agent. Mesoporous-silica-coated $NaYF_4$:Yb/Tm nanoparticles with a core/shell

View Article Online
DOI: 10.1039/C6RA23440B

structure were fabricated and used as drug carriers and photo-transducers for PDT treatment. The emission of UCNP was used to excite the PS, as shown in **Fig. 2**. RTA molecules were incorporated into the mesoporous silica shell and the fluorescent emission from the UCNP can be absorbed by RTA molecules coated on their surfaces under NIR irradiation. Subsequently, the excited RTA molecules interact with surrounding ground-state molecular oxygen for the generation of ROS, leading to oxidative damage of cancer cells.

2. Experimental section

2.1. Chemicals and reagents

Riboflavin (RF), 2,2,6,6-tetramethyl-4-piperidone (4-oxo-TEMP), 5,5-dimethyl-1-pyrroline-N-oxide (DMPO), catalase, yttrium chloride (YCl_3, 99%), ytterbium chloride ($YbCl_3$, 99%), thulium chloride ($TmCl_3$, 99%), octadecene (ODE), ammonium fluoride (NH_4F), octadecyltrimethoxysilane ($C_{18}TMS$), tetraethyl orthosilicate (TEOS), oleic acid, igepal CO-520 and cyclohexane were purchased from Sigma-Aldrich Co. (USA). Ferrous sulfate heptahydrate ($FeSO_4.7H_2O$), sodium hydroxide (NaOH), hydrochloric acid (HCl), dimethyl sulfoxide (DMSO), acetic anhydride, HPLC-grade acetic acid, and HPLC-grade ammonium acetate were purchased from Shanghai Chemical Reagent Co. (China). HPLC-grade methanol was purchased from Merck Inc. (Germany). Ultrapure (MilliQ Inc., USA) water (resistivity of 18.2 MΩ-cm) was used in the experiments. All chemicals were of analytical grade (or HPLC-grade) and used without further purification.

View Article Online
DOI: 10.1039/C6RA23440B

RTA, a synthetic derivative of RF, was prepared through a easy-to-operated esterification process of RF with acetic anhydride (**Scheme 1**).[34, 46-48] In brief, RF (5.0 g) was suspended in acetic anhydride solution (50 mL), then added sulfuric acid (0.1 mL) to initiate the esterification reaction, and magnetic stirred at 80°C for 4 h under argon atmosphere. The cooled solution was neutralized with 1.0 M $NaHCO_3$ (200 mL), extracted with CH_2Cl_2 and washed with ultrapure water. The organic layer was dried with anhydrous magnesium sulfate, and evaporated under reduced pressure. The raw product was further recrystallized from MeOH/H_2O (4:1; v/v) to yield pure RTA.

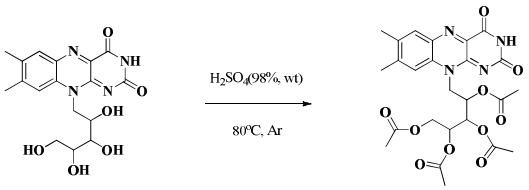

Scheme. 1. Schematic representation of synthetic procedure to obtain 2',3',4',5'-tetraacetylriboflavin (RTA) from riboflavin (RF).

A LTQ XL orbitrap high resolution mass spectrometry (Thermo Fisher Sci. Inc., USA), coupled with an electrospray ionization (ESI) source, was used for direct injection ESI-MS analysis. Data acquisition was performed with Xcalibur 2.0 software (Thermo Fisher Sci. Inc., USA). The spray voltage was set to 5.0 kV, capillary temperature to 280°C. The sheath and auxiliary gas flow rate (both nitrogen) were set at 18 and 3 arbitrary units, respectively. Full MS scans were acquired in the orbitrap analyzer in a positive mode with the resolution set to a value of 60000. ^{1}H-NMR spectrum were collected using a Agilent 600 MHz NMR spectrometer (Agilent Inc., USA). FTIR spectrum of RTA was recorded on a VERTEX 70 FT-IR spectrometer (Bruker Inc., Germany) operated at a setting of 32 scans at a spectral resolution of 4 cm^{-1}. **Analysis data: HR-MS** (ESI) *m/z* calculated for $C_{25}H_{29}N_4O_{10}$

View Article Online
DOI: 10.1039/C6RA23440B

$[M+H]^+$ 545.1883, experimental found 545.1879. **^{1}H-NMR** (600 MHz, DMSO-d6, ppm): 10.32 (s, 1H, Ar-NH), 7.88 (s, 1H, Ar-H), 7.72 (s, 1H, Ar-H), 5.46 (m, 1H, -CHOAc), 5.33 (m, 1H, -CHOAc), 4.83 (m, 1H, -CHOAc), 4.36-4.25 (d, 2H, $-CH_2OAc$), 4.22-4.15 (dd, 2H, -CHH), 2.50 (s, 3H, Ar-CH_3), 2.45 (s, 3H, Ar-CH_3), 2.38 (s, 3H, -$COOCH_3$), 2.18 (s, 3H, -$COOCH_3$), 1.98 (s, 3H, -$COOCH_3$), 1.60 (s, 3H, -$COOCH_3$). **FT-IR** (neat KBr): ν (cm^{-1}) = 3200 (br), 3029(m), 1745 (m), 1668 (s), 1370 (s), 1509 (s), 1360 (s), 1231 (vs), 1171 (vs), 1035 (s), 850 (vs).

2.2. Electrochemical analysis of RTA

Cyclic voltammetry (CV) and differential pulse voltammetry (DPV) tests were conducted in a 3-electrode system with a CHI 660C electrochemical workstation (Chenhua Instrument Co., China). The system utilized glassy carbon (GC) electrode as working electrode, KCl-saturated Ag/AgCl as reference electrode, platinum wire as counter electrode. Before each test, the GC electrode (d = 3 mm) was polished with 0.3- and 0.05-μm alumina powder in succession, and sonicated in water for 30 seconds. The electrolyte, consisted of 100 μM RTA in 100 mM PBS (pH 7.0), was deoxygenated by nitrogen prior to the electrochemical tests. All experiments were conducted at ambient temperature of 25°C.

2.3. Synthesis of mesoporous silica-coated $NaYF_4$:Yb/Tm nanoparticles

$NaYF_4$:Yb/Tm nanoparticles were fabricated and used as photo-transducers in this study. $NaYF_4$:Yb/Tm nanocrystals with uniform size distribution were synthesized via an efficient and user-friendly method.[41,42] $NaYF_4$:Yb(18%)/Tm(2%) nanocrystals were synthesized following a protocol that was reported previously.[16, 41] YCl_3 (0.8 mmol), $YbCl_3$ (0.18 mmol), and $TmCl_3$ (0.02 mmol) were mixed with 12

View Article Online
DOI: 10.1039/C6RA23440B

mL oleic acid and 15 mL octadecene (ODE) in a 50 mL flask. The solution was heated to 160°C to form a homogeneous solution, and then cooled to ambient temperature (25°C). A 10 mL methanol solution containing NaOH (2.5 mmol) and NH_4F (4 mmol) was slowly added into the flask and stirred for 30 min. The solution was slowly heated to remove methanol, degassed at 100°C for 10 min, and then heated to 300°C and maintained for 2.0 h under argon protection. After the solution was cooled naturally, nanocrystals were precipitated from the solution with ethanol and washed with ethanol/water (1:1 v/v) three times.

Porous silica-coated $NaYF_4$:Yb/Tm nanoparticles were further achieved successfully by one pot facile synthetic process.[39] Octadecyltrimethoxysilane (C_{18}TMS) was used as soft template, which has been used for preparing hydrophobic coatings and self-assembled monolayers. Briefly, CO-520 (1.0 mL), cyclohexane (6.0 mL) and $NaYF_4$:Yb/Tm nanocrystal solution in cyclohexane (40 mL, 0.01 M) were mixed and stirred for 60 min. Then, 1.0 mL ammonia (28 wt%) was added into the previous solution and sonicated for 30 min until a transparent emulsion was formed. The mixture solution of 120 μL TEOS and 50 μL octadecyltrimethoxysilane (C_{18}TMS) was then added into the previous solution. Finally, the solution was stirred for 48 h at a speed of 800 rpm at ambient temperature of 25°C. Silica-coated $NaYF_4$:Yb/Tm nanoparticles were collected by centrifugation after precipitation by adding acetone, washed with ethanol three times and finally dried at 60°C for 10 h. The as-prepared sample was calcinated at 500°C in static air with a heating rate of 1.0°C/min and a dwelling time of 2.0 h.

Mesoporous-silica-coated $NaYF_4$:Yb/Tm nanoparticles (20 mg) were soaked in aqueous solutions of PSs (RTA or RF, 50 mL, 10 μg/mL) for 24 h at ambient temperature (25°C). The nanoparticles were then collected by centrifugation (5000 g,

View Article Online
DOI: 10.1039/C6RA23440B

5 min) and washed with phosphate buffer saline solution (PBS, 0.02 M, pH=7.40). Initial and residual concentrations of PSs were analyzed using a high performance liquid chromatography system (HPLC-1100, Agilent Inc., USA) equipped with a VWD detector and a Hypersil ODS column. A mixture of methanol and water (30:70, v/v) was used as the isocratic mobile phase with 0.1% acetic acid in water. The flow rate was set at 1.0 mL/min, the UV detector was set at 360 nm, and the column temperature was set at 30°C.

The morphology and size of the as-prepared samples were investigated by transmission electron microscopy (TEM, JEOL 3010, JEOL Co., Japan). UV-visible absorption spectra were performed using a UV-visible spectrometry (UV-2450, Shimadzu Co., Japan). The spectra were collected from 200 nm to 800 nm by an increment of 0.5 nm. All measurements were performed in standard 10 mm quartz cuvettes. Excitation–emission matrix fluorescence spectroscopic analysis was performed using a luminescence spectrometry (LS-55, Perkin-Elmer Co., USA) equipped with a 980 nm excitation source. Fluorescence spectra were collected with subsequent scanning emission spectra from 200 to 800 nm by an increment of 0.5 nm under the 980 nm-excitation.

2.4. Photostability analysis of RTA

The photostabilities of RTA and RF under both visible and NIR irradiation were evaluated in aqueous solutions (pH=7.0). A 50-W Xe-arc lamp (XD-300, Nanjing Yanan Co., China) equipped with an UV-cutoff (>400 nm) was used as visible light source and a 980 nm NIR laser (MDL-980, Changchun New industries optoelectronics tech. Co., China) was used as NIR light source. Samples were

View Article Online
DOI: 10.1039/C6RA23440B

irradiated, and aliquots were removed and analyzed at given time intervals (10 min). The light dependence processes were monitored and analyzed using both high performance liquid chromatography (HPLC-1100, Agilent Inc., USA) and UV-visible spectrometry (UV-2450, Shimadzu Co., Japan).

2.5. ROS detection using electron paramagnetic resonance spectroscopy

EPR spectra were obtained using a JEOL JES-FA200 EPR spectrometer (JEOL Co., Japan) with a 500-W Xe-arc lamp equipped with an UV-cutoff (>400 nm) as visible-light source and a 980-nm laser with an output power of 1000 mW as a near-infrared (NIR) light source. Spectrometer with X-band microwave frequency of 9.072 GHz, microwave power of 2.02 mW, spectral window of 100 G, and modulation amplitude of 1.00 G was used at ambient temperature of 25°C. 4-oxo-TEMP was used to detect $^{1}O_2$, and DMPO was utilized to measure $O_2^{\bullet-}$ and •OH.[35, 36, 50-53]

$^{1}O_2$ was detected with the EPR method using 4-oxo-TEMP as a spin-trapping reagent (Reaction 1).[35, 50] Solutions of RTA were prepared in ultrapure water. Under visible irradiation, the incubation of RTA at 100 μM with the spin-trapping agent 4-oxo-TEMP of 100 mM resulted in the formation of a adducts. 200 μL of the freshly prepared mixture was added to a quartz EPR tube and illuminated for 0, 1.0, 2.0, 3.0, 4.0, and 5.0 min before recording the EPR spectra. Under NIR-irradiation, the incubation of RTA/UCNP (5 mg/mL) with the spin-trapping agent 4-oxo-TEMP of 100 mM resulted in the formation of the adducts of 4-oxo-TEMP/$^{1}O_2$. 200 μL of the freshly prepared mixture was added to a quartz EPR tube and illuminated for 10 min before recording the EPR spectra. The generation of $^{1}O_2$ was detected as an EPR signal, because 4-oxo-TEMPO is formed by the reaction of $^{1}O_2$ with 4-oxo-TEMP.

View Article Online
DOI: 10.1039/C6RA23440B

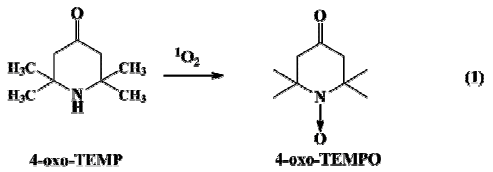

DMPO was used as a spin-trapping agent for the detection of $O_2^{\bullet-}$ (Reaction 2).[35, 36,50] Solutions of RTA were prepared in DMSO. Under visible irradiation, the incubation of 100 μM RTA with 100 mM spin-trapping agent DMPO resulted in the formation of the radical adducts. 200 μL of the freshly prepared mixture was added to a quartz EPR tube and illuminated for 0, 0.5 ,1.0, 1.5, and 2.0 min before recording the EPR spectra. Under NIR-irradiation, the incubation of RTA/UCNP (5 mg/mL) with 100 mM spin-trapping agent DMPO resulted in the formation of the radical adducts. 200 μL of the freshly prepared mixture was added to a quartz EPR tube and illuminated for 10 min before recording the EPR spectra.

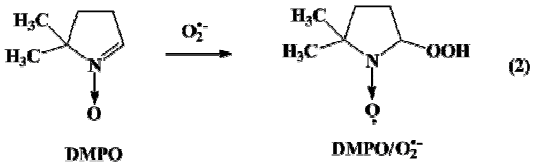

DMPO was also used as a spin-trapping agent for the detection of HO• (Reaction 3).[36, 51, 52] Solutions were prepared in ultrapure water. Under visible irradiation, the incubation of RTA (100 μM) and $FeSO_4$ (10 μM) with 100 mM spin-trapping agent DMPO resulted in the formation of the radical adducts. Then, 200 μL of the freshly prepared mixture was added to a quartz EPR tube and illuminated for 0, 1.0, 2.0, and 3.0 min before recording the EPR spectra. Under NIR-irradiation, the incubation of RTA/UCNP (5 mg/mL) and $FeSO_4$ (2 μM) with 100 mM spin-trapping agent DMPO resulted in the formation of the radical adducts. Then, 200 μL of the freshly prepared mixture was added to a quartz EPR tube and illuminated for 10 min before recording the EPR spectra.

View Article Online
DOI: 10.1039/C6RA23440B

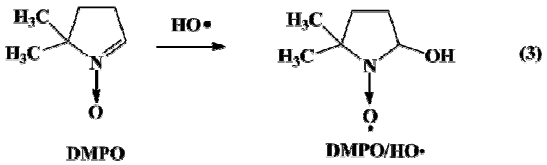

2.6. Cell culture and in-vitro PDT test

In-vitro cytotoxicity assays were further performed using the human breast cancer cell line MDA-MB-231 from the American Type Culture Collection (ATCC). MDA-MB-231cells were cultured in RPMI 1640 medium, supplemented with 10% fetal bovine serum and 2 mM L-glutamine at 37°C using a humidified 5% CO_2 incubator. The MDA-MB-231 cells were seeded onto 96-well plates at 2.0×10^3 cells per well and further incubated for 24 h. The culture medium was then replaced with 100 μL of freshly prepared culture medium containing either free PS or PS/UCNP at different concentrations.

Cells were treated with free RF, RTA, RF/UCNP or RTA/UCNP composites and incubated for 24 h and then exposed to visible or 980 nm-NIR irradiation. All cells were then incubated for another 48 h at 37°C and evaluated by MTT viability assay. For MTT assay, MDA-MB-231 cancer cells were collected and diluted to a cell density of 1×10^5/mL in complete medium, and then seeded into 96-well plates (100 μL/well). After being cultured for 24 h, the nanoparticles with different concentrations (0.625, 1.25, 2.5, and 5.0 mg/mL) with and without PS were added to the cells and the cells were incubated for 24 h at 37°C. The exposure time of NIR-irradiation was divided into several sections (2 min per section) to avoid the over-heating possibility. The cells were then incubated at 37°C for 48 h. The cell viability was measured by MTT assay (3-(4,5-dimethylthiazol-2-yl)-2,5-diphenyl tetrazoliumbromide) and expressed as a percentage of the control.

View Article Online
DOI: 10.1039/C6RA23440B

3. Results and Discussion

3.1. Electrochemical characteristics of RTA

The known ability of isoalloxazine ring to act as an excellent PS has been supposed to play a key role in the generation of $^1O_2$ or $O_2^{\bullet-}$. In our previous study, RF has been reported to play a dual role of excellent PS and effective electron mediator in the process of •OH generation.[35, 36] Some PSs have been shown to produce different kind ROS, and synergistic effects of $^1O_2$ and •OH on PDT treatment has been proposed.[17] However, RF is susceptible to photodegradation, likely due to the instability of the ribose chain. Chemical modification of the ribose chain of the molecule is highly desired, and can improve the yield and lifetime of the triplet state and result in a more photostable derivative.[34, 47-49] RTA was synthesized through a easy-to-operated esterification process of RF with acetic anhydride. The electron shuttling capacity of RF as a redox-active molecule paly a key role in the generation of $O_2^{\bullet-}$ or •OH. Thus, electrochemical characterization of RTA and RF were fristly conducted to analysis of their oxidation-reduction potentials.

The sterile glassy carbon electrodes were exposed to 0.05 mM RF. CV analysis was performed at a scan rate of 100 mV/s. The potential difference between oxidation and reduction peaks was 58 mV and the centers of the reversible voltammetric peaks were at -0.40V (**Fig. 3A**). These results show the oxidation-reduction process of RF is reversible and RF could be used as a mediator in electron transfer process. To test the redox property of RTA, CV experiments were conducted in RTA solution. Compared to the blank electrolyte (PBS solution), RTA shows a pair of obvious reversible redox peaks with potential difference between oxidation and reduction peaks was 49 mV, and the centers of the reversible voltammetric peaks were at -0.37 V. The redox peaks

View Article Online
DOI: 10.1039/C6RA23440B

of RTA were more positive than that of RF, which was consistent with DPV results (**Fig. 3B**). The DPV results show that the redox potential of RTA was larger than that of RF by 30 mV. These results indicate that RTA was more easily to be reduced. Additionally, the peak separation of RTA was also smaller, suggesting that RTA was more electrochemically reversible than RF. These results demonstrate that RTA was successfully synthesized from RF and its electrochemical properties were improved after the modification.

3.2. Characteristics of $NaYF_4$:Yb/Tm upconversion nanoparticles

TEM analysis was used to examine the morphology of the UCNP nanoparticles. The results clear show that the nanoparticles were discrete and uniform with an average diameter of 30 and 50 nm for $NaYF_4$:Yb/Tm (**Fig. 4A**) and porous silica-coated $NaYF_4$:Yb/Tm (**Fig. 4B**), respectively. Brunauer–Emmet–Teller (BET) analysis reveal mesoporous structure of silica-coated $NaYF_4$:Yb/Tm with an average pore-size distribution of 2.30 nm and a specific surface area of 680 m^2/g. Mesoporous-silica-coated $NaYF_4$:Yb/Tm nanoparticles (100 mg) were soaked in PS aqueous solution (RF or RTA, 100 mL, 0.1 mM) for 24 h at ambient temperature of 25°C. The nanoparticles were then collected by centrifugation and washed with PBS solution (0.02 M, pH=7.4). Concentrations of PS solutions (RTA or RF) were determined using HPLC method and the amount of adsorbed into the mesoporous silica was about 2.0 wt%.

3.3. Emission spectrum analysis of $NaYF_4$:Yb/Tm nanoparticles and absorbance spectrum analysis of RTA

The luminescent spectrum of $NaYF_4$:Yb/Tm nanoparticles and the UV-visible absorption spectrum of the RTA and RF solutions were further analyzed. The

View Article Online
DOI: 10.1039/C6RA23440B

luminescence spectrum of the mesoporous silica-coated $NaYF_4$:Yb/Tm upon NIR-irradiation (980 nm) is shown in Fig. 5A. The dominant emissions are located at 345, 360, 451, and 476 nm. As shown in Fig. 5B, there is a good overlap between the fluorescence emission of $NaYF_4$:Yb/Tm nanoparticles and the UV-visible absorption of RTA and RF solutions (main peaks located at 372 and 450 nm). It is envisaged that the PS (RTA or RF) can be aborted and activated by the UCNP to produce ROS and kill cancer cells when exposed to NIR irradiation.

3.4. Photostability analysis of RTA

Qualitative evaluation of the photostabilities of RTA and RF were performed under visible or NIR (980 nm, 500 mw) irradiation. Initial and residual concentrations of RTA and RF were analyzed using HPLC. Free RF in solution was degraded completely after one hour of visible irradiation, while RTA was degraded only 20% under similar conditions. Compared with visible irradiation, both free RTA and RF, and in the form of PS/UCNP nanocomposites exhibit an appreciable photostability under NIR irradiation, as shown in **Fig. 6**. These results indicate that the RTA molecule in the form of RTA/UCNP nanocomposite has a good photostability under NIR irradiation, and could used as a potential candidate of PS for PDT applications.

3.5. Analysis of ROS using electron paramagnetic resonance spectroscopy

ROS generation during the NIR-triggered photosensitization process RTA was analyzed using EPR spectroscopy combined with spin trapping. Solution of RTA/UCNP (5 mg/mL) with DMPO (100 mM) was prepared in ultrapure water (pH=3.0). 4-oxo-TEMP was used to detect $^1O_2$, and DMPO was utilized to measure $O_2^{\bullet-}$ and •OH.[51, 52] 200 μL of this freshly prepared mixture was added to a quartz EPR

View Article Online
DOI: 10.1039/C6RA23440B

tube and illuminated for 5.0 min before recording the EPR spectra. The specific signals of 4-oxo-TEMP/$^1O_2$ were produced by $^1O_2$ generated from photoexcited RTA (**Fig. 7A**). The spectrum is composed of a triplet of lines, with a peak height ratio of 1:1:1, with parameters including hyperfine constants, a_N=16.30 G and a g-value=2.0055. These parameters exactly matched with accurate EPR spectrum simulation of 4-oxo-TEMP/$^1O_2$. $O_2^{\bullet-}$ is sensitive to the presence of proton and its lifetime is very short in protic solvents.[35, 36] Thus, it is difficult to detect $O_2^{\bullet-}$ in protic solvent and an aprotic solvent of DMSO was used in this study to facilitate $O_2^{\bullet-}$ detection.[51,53] The hyperfine splitting constants for DMPO/$O_2^{\bullet-}$ were a_N=12.80 G; a_H^{β}=10.41 G; a_H^{γ}=1.35 G; g=2.0021 (**Fig. 7B**). An accurate EPR spectrum simulation of DMPO/$O_2^{\bullet-}$ has also been performed.

On the basis of the analysis of both $O_2^{\bullet-}$ and $^1O_2$, we further examined the feasibility of NIR-initiated •OH generation of RTA solution in the presence of dissolved-iron. Solution of RTA/UCNP (5 mg/mL) and $FeSO_4$ (5 μM) with DMPO (100 mM) was prepared in acidic water (pH=3.0). Upon exposure to NIR irradiation, a major radical/DMPO adduct was formed and assigned to DMPO/•OH. The hyperfine splitting constants for DMPO/•OH were a^H=a^N=14.96 G and a g-value=2.0050 (**Fig. 7C**). Among the signals for DMPO/•OH (1:2:2:1), a weak EPR signal was composed of a triplet of lines with a peak height ratio of 1:1:1. There is a signal of oxidized DMPO (DMPOX) in the EPR spectra. Similar results of ROS generation were obtained with RF/UCNP solution under NIR irradiation.

3.6. In-vitro PDT activity of RTA/UCNP nanocomposites

As designed, the NIR-triggered release of ROS from RTA/UCNP nanocomposites was deemed to exhibit the spatio-temporal controlled anticancer

View Article Online
DOI: 10.1039/C6RA23440B

effects. Therefore, the therapeutic potential of RTA/UCNP composite was evaluated *in-vitro* using the human breast cancer cell. Cells with free RTA or RF (10 μg/mL) were exposed to a 50-W Xe-arc lamp equipped with an UV-cutoff (>400 nm). The cell viability with different exposure time to visible irradiation (5, 10, 20, and 30 min) indicated that the cell viability decreased with the exposure time under visible irradiation, suggesting an increased amount of ROS produced by the PS (RTA or RF). Normal incubated cells was used as control (Control-1). Cells incubated without visible irradiation show that both RF (Control-2) and RTA (Control-3) are nontoxic and biocompatible. Cells of control-4 were incubated under visible irradiation without adding any PS. RTA has a much better PDT effect than RF, which can be attributed to the improved photostability of RTA. The results of the control tests show that PS and visible irradiation were both required.

Fig. 8A shows the effect of exposure time to NIR irradiation on the cell viability in the presence of RTA/UCNP or RF/UCNP (5 mg/mL). Cells cultured with PS/UCNP were exposed to a 980 nm-NIR-laser with an output power of 500 mW. The cell viability of cancer cells clearly decreased with increasing irradiation time. Control experiments with NIR irradiation in the absence of PS/UCNP also showed that NIR irradiation alone did not initiate cell death. **Fig. 8B** showed that the viability of cells incubated with the amount of RTA/UCNP (0.625, 1.25, 2.5, and 5 mg/mL) exposed to NIR irradiation for 30-min was significantly lower as compared to the nanoparticles without RTA/UCNP (Control-1) or without NIR irradiation (Control-2). Similar results were obtained with RF/UCNP solution under NIR irradiation.

Fig. 8C shows the effect of Fe^{2+} on the cell viability. At a low concentration range (0-1.0 μg/mL), the cell viability decreased with an increase of Fe^{2+} concentration. Interestingly, the adding of Fe^{2+} facilitates the generation of •OH, and

View Article Online
DOI: 10.1039/C6RA23440B

results in a increase of phototoxicity. Howerver, with Fe^{2+} concentration further increased, the cell viability increased with increasing Fe^{2+} concentration.

4. Conclusions

In summary, a novel NIR-light-triggered PDT nanosystem has been developed using an old vitamin (VB_2) integrated with the upconversion nanotechnology. Mesoporous-silica-coated $NaYF_4$:Yb/Tm nanoparticles were successfully fabricated, which played a dual role of drug carrier and photo transducer. Chemical modification of this old vitamin was performed through a easy-to-operated esterification process to improve its photostability. This nanoplatform has some desired features for an ideal PDT drug, including: (1) high water-solubility; (2) excellent photochemical reactivity to produce reactive oxygen species; (3) low dark toxicity; and (4) can be excited at NIR region where tissue penetration of irradiation is at a maximum. The results of *in-vitro* cell experiment demonstrate that RTA/UCNP nanocomposite of the proposed design has great potential in PDT application.

Acknowledgements

The authors wish to thank the National Science Foundation of China (No.21207031, No.21471043), the China Postdoctoral Science Foundation (No. 2016M592049), and the Key Laboratory of Urban Pollutant Conversion, Chinese Academy of Sciences (No. KF201603) for the support of this study.

View Article Online
DOI: 10.1039/C6RA23440B

References

1 D. E. Dolmans, D. Fukumura and R. K. Jain, Photodynamic therapy for cancer, *Nat. Rev. Cancer*, 2003, **3**, 380-387.

2 R. S. Balaban, S. Nemoto and T. Finkel, Mitochondria, oxidants, and aging, *Cell*, 2005, **120**, 483-495.

3 K. Ishikawa, K. Takenaga, M. Akimoto, N. Koshikawa, A. Yamaguchi, H. Imanishi, K. Nakada, Y. Honma and J. Hayashi, ROS-generating mitochondrial DNA mutations can regulate tumor cell metastasis, *Science*, 2008, **320**, 661-664.

4 W. M. Sharman, C. M. Allen and J. E. van Lier, Photodynamic therapeutics: basic principles and clinical applications, *Drug Discov. Today*, 1999, **4**, 507-517.

5 P. Mroz, A. Pawlak, M. Satti, H. Lee, T. Wharton, H. Gali, T. Sarna and M. R. Hamblin, Functionalized fullerenes mediate photodynamic killing of cancer cells: Type I versus Type II photochemical mechanism, *Free Radical Bio. Med.*, 2007, 43, 711-719.

6 Y. Arenas, S. Monro, G. Shi, A. Mandel, S. McFarland and L. Lilge, Photodynamic inactivation of *Staphylococcus aureus* and methicillin-resistant *Staphylococcus aureus* with Ru(II)-based type I/type II photosensitizers, *Photodiagn. Photodyn. Ther.*, 2013, **10**, 615-625.

7 M. Ochsner, Photophysical and photobiological processes in the photodynamic therapy of tumors, *J. Photochem. Photobiol. B Biol.*, 1997, **39**, 1-18.

8 L. Li, G. Ishdorj and S. B. Gibson, Reactive oxygen species regulation of autophagy in cancer: Implications for cancer treatment, *Free Radical Bio. Med.*, 2012, **53**, 1399-1410.

View Article Online
DOI: 10.1039/C6RA23440B

9 F. Cieplik, A. Späth, J. Regensburger, A. Gollmer, L. Tabenski, K. Hiller, W. Bäumler, T. Maisch and G. Schmalz, Photodynamic biofilm inactivation by SAPYR-An exclusive singlet oxygen photosensitizer, *Free Radical Bio. Med.*, 2013, **65**, 477-487.

10 Y. Yamakoshi, N. Umezawa, A. Ryu, K. Arakane, N. Miyata, Y. Goda, T. Masumizu and T. Nagano, Active oxygen species generated from photoexcited fullerene (C_{60}) as potential medicines: $O_2^{\bullet-}$ versus $^1O_2$, *J. Am. Chem. Soc.*, 2003, **125**, 12803-12809.

11 A. Montazerabadi, A. Sazgarnia, M. H. Bahreyni-Toosi, A. Ahmadic, A. Shakeri-Zadeh and A. Aledavood, Mitoxantrone as a prospective photosensitizer for photodynamic therapy of breast cancer, *Photodiagn. Photodyn. Ther.*, 2012, **9**, 46-51.

12 A. Nadhman, S. Nazir, M. I. Khan, S. Arooj, M. Bakhtiar, G. Shahnaz and M. Yasinzai, PEGylated silver doped zinc oxide nanoparticles as novel photosensitizers for photodynamic therapy against Leishmania, *Free Radical Bio. Med.*, 2014, **77**, 230-238.

13 W. J. Yan, Q. Wang, C. H. Yuan, F. Wang, Y. Ji, F. Dai, X. L. Jin and B. Zhou, Designing piperlongumine-directed anticancer agents by an electrophilicity-based prooxidant strategy: A mechanistic investigation, *Free Radical Bio. Med.*, 2016, **97**, 109-123.

14 M. Rajendran, Quinones as photosensitiser for photodynamic therapy: ROS generation, mechanism and detection methods, *Photodiagn. Photodyn. Ther.*,

View Article Online
DOI: 10.1039/C6RA23440B

2016, **13**, 175-187.

15 C. S. Lee, W. Park, Y. U. Jo and K. Na, A charge-switchable, four-armed polymeric photosensitizer for photodynamic cancer therapy, *Chem. Commun.*, 2014, **50**, 4354-4357.

16 F. Xu, L. Ding, W. Tao, X. Z. Yang, H. S. Qian and R. S. Yao, Mesoporous-silica-coated upconversion nanoparticles loaded with vitamin B_{12} for near-infrared-light mediated photodynamic therapy, *Materials Lett.*, 2016, **167**, 205-208.

17 J. M. Dąbrowski, L. G. Arnaut, M. M. Pereira, K. Urbańska, S. Simões, G. Stochel and L. Cortes, Combined effects of singlet oxygen and hydroxyl radical in photodynamic therapy with photostable bacteriochlorins: Evidence from intracellular fluorescence and increased photodynamic efficacy *in vitro*, *Free Radical Bio. Med.*, 2012, **52**: 1188-1200.

18 X. Chen, L. Hui, D. A. Foster and C. M. Drain, Efficient synthesis and photodynamic activity of porphyrin-saccharide conjugates: Targeting and incapacitating cancer cells, *Biochemistry*, 2004, **43**, 10918-10929.

19 I. Lanzo, N. Russo and E. Sicilia, First-principle time-dependent study of magnesium-containing porphyrin-like compounds potentially useful for their application in photodynamic therapy, *J. Phys. Chem. B*, 2008, **112**, 4123-4130.

20 J. F. Lovell, M. W. Chan, Q. C. Qi, J. Chen and G. Zheng, Porphyrin FRET acceptors for apoptosis induction and monitoring, *J. Am. Chem. Soc.*, 2011, **133**, 18580-18582.

21 X. C. Zhu, W. T. Lu, Y. Z. Zhang, A. Reed, B. Newton, Z. Fan, H. T. Yu, P. C.

View Article Online
DOI: 10.1039/C6RA23440B

Ray and R. M. Gao, Imidazole-modified porphyrin as a pH-responsive sensitizer for cancer photodynamic therapy, *Chem. Commun.*, 2011, **47**, 10311-10313.

22 T. C. Lei, G. F. Glazner, M. Duffy, L. Scherrer, S. Pendyala, B. H. Li, X. L. Wang, H. W. Wang and Z. Huang, Optical properties of hematoporphyrin monomethyl ether (HMME), a PDT photosensitizer, *Photodiagn. Photodyn. Ther.*, 2012, **9**, 232-242.

23 R. Dosselli, C. Tampieri, R. Ruiz-González, S. De Munari, X. Ragàs, D. Sánchez-García, M. Agut, S. Nonell, E. Reddi and M. Gobbo, Synthesis, characterization, and photoinduced antibacterial activity of porphyrin-type photosensitizers conjugated to the antimicrobial peptide apidaecin 1b, *J. Med. Chem.*, 2013, **56**, 1052-1063.

24 E. Alves, M. A. F. Faustino, M. G. P. M. S. Neves, Â. Cunha, H. Nadais and A. Almeida, Potential applications of porphyrins in photodynamic inactivation beyond the medical scope, *J. Photochem. Photobiol., C: Photochem. Rev.*, 2015, **22**, 34-57.

25 T. Rodrigues, D. Reker, P. Schneider and G. Schneider, Counting on natural products for drug design, *Nat. Chem.*, 2016, **8**, 531-541; 2016.

26 T. A. Shell and D. S. Lawrence, A new trick (hydroxyl radical generation) for an old Vitamin (B_{12}), *J. Am. Chem. Soc.*, 2011, **133**, 2148-2150.

27 T. A. Shell, J. R. Shell, Z. L. Rodgers and D. S. Lawrence, Tunable visible and near-IR photoactivation of light-responsive compounds by using fluorophores as light-capturing antennas, *Angew. Chem. Int. Ed.*, 2014, **53**, 875-878.

View Article Online
DOI: 10.1039/C6RA23440B

28 H. Canstein, J. Ogawa, S. Shimizu and J. R.Lloyd, Secretion of flavins by *Shewanella* species and their role in extracellular electron transfer, *Appl. Environ. Microb.*, 2008, **7**, 615-623.

29 E. Marsili, D. B. Baron, I. D. Shikhare, D. Coursolle, J. A. Gralnick and D. R. Bond, *Shewanella* secretes flavins that mediate extracellular electron transfer, *Proc. Natl. Acad. Sci. USA,* 2008, **105**, 3968-3973.

30 S. Sanudo-Wilhelmy, L. S. Cutter, R. Durazo, E. A. Smail, L. Gomez-Consarnau, E. A. Webb, M. G. Prokopenko, W. M. Berelson and . Karl, ultiple B-vitamin depletion in large areas of the coastal ocean, *Proc. Natl. Acad. Sci. USA,* 2009, **109**,14041-14045.

31 S. Babanova, O. Bretschger, J. Roy, A. Cheung, K. Artyushkova and P. Atanassov, Innovative statistical interpretation of *Shewanella oneidensis* microbial fuel cells data *Phys. Chem. Chem. Phys.*, 2014,**16**, 8956-8969.

32 Y. Barbieri, W. A. Massad, D. J. Diaz, J. Sanz, F. Amat-Guerri and N. A. Garcia, hotodegradation of bisphenol A and related compounds under natural-like conditions in the presence of riboflavin: Kinetics, mechanism and photoproducts, *Chemosphere*, 2008, **73**, 564-571.

33 E. Haggi, S. Bertolotti and N. A. Garcia, Modelling the environmental degradation of water contaminants. Kinetics and mechanism of the riboflavin-sensitised-photo oxidation of phenolic compounds, *Chemosphere*, 2004, **5**, 1501-1507.

34 C. K. Remucal and K. McNeill, Photosensitized amino acid degradation in the

View Article Online
DOI: 10.1039/C6RA23440B

presence of riboflavin and its derivatives, *Environ. Sci. Technol.*, 2011, **45**, 5230-5237.

35 F. Xu, X. N. Song, G. P. Sheng, H. W. Luo, W. W. Li, R. S. Yao and H. Q. Yu, Sunlight-mediated degradation of methyl orange sensitized by riboflavin: Roles of reactive oxygen species, *Sep. Purif. Technol.*, 2015, **142**, 18-24.

36 F. Xu, X. N. Song, G. P. Sheng, H. W. Luo, W. W. Li, R. S. Yao and H. Q. Yu, Vitamin B_2-initiated hydroxyl radical generation under visible light in the presence of dissolved iron, *ACS Sustainable Chem. Eng.*, 2015, **3**, 1756-1763.

37 Y. Suzuki, Y. Kitatsuji, T. Ohnuki and S. Tsujimura, Flavin mononucleotide mediated electron pathway for microbial U(VI) reduction, *Phys. Chem. Chem. Phys.*, 2010,**12**, 10081-10087.

38 E. Kosarieh, S. S. Khavas, A. Rahimi, N. Chiniforush and N. Gutknecht, The comparison of penetration depth of two different photosensitizers in root anal s with and without smear layer: An in vitro study, *Photodiagn. Photodyn. Ther.*, 2016, **13**,10-14.

39 S. Kishimoto, M. Bernardo, K. Saito, S. Koyasu, J. B. Mitchell, P. L. Choyke and M. C. Krishn, Evaluation of oxygen dependence on in vitro and in vivo cytotoxicity of photoimmunotherapy using IR-700-antibody conjugates, *Free Radical Bio. Med.*, 2015, **85**, 24-32.

40 D. Gao, R. R. Agayan, H. Xu, M. A. Philbert and R. Kopelman, Nanoparticles for two-photon photodynamic therapy in living cells, *Nano Lett.*, 2006, **6**, 2383-2386.

41 H. S. Qian, H. C. Guo, P. C. L. Ho, R. Mahendran and Y. Zhang,

View Article Online
DOI: 10.1039/C6RA23440B

Mesoporous-silica-coated up-conversion fluorescent nanoparticles for photodynamic therapy, *Small*, 2009, **5**, 2285-2290.

42 B. B. Ding, H.Y. Peng, H. S. Qian, L. Zheng and S. H. Yu, Unique upconversion core-shell nanoparticles with tunable fluorescence synthesized by a sequential growth process, *Adv. Mater. Interfaces*, 2016, **3**, 1500649.

43 P. Zhang, W. Steelant, M. Kumar and M. Scholfield, Versatile photosensitizers for photodynamic therapy at infrared excitation, *J. Am. Chem. Soc.*, 2007, **129**, 4526-4527.

44 A. V. Kachynski, A. Pliss, A. N. Kuzmin, T. Y. Ohulchanskyy, A. Baev, J. Qu and P. N. Prasad, Photodynamic therapy by in situ nonlinear photon conversion, *Nat. Photon.*, 2014, **8**, 455-461.

45 G. F. Wang, Q. Peng and Y. D. Li, Lanthanide-doped nanocrystals: synthesis, optical-magnetic properties, and applications, *Acc. Chem. Res.*, 2011, **44**, 322-332.

46 L. Z. Zhao, J. J. Peng, Q. Huang, C. Y. Li, M. Chen,Y. Sun, Q. N. Lin, L. Y. Zhu and F. Y. Li, Near-infrared photoregulated drug release in living tumor tissue via yolk-shell upconversion nanocages, *Adv. Funct. Mater.*, 2014, **24**, 363-371.

47 E. C. Smith and D. E. Metzler, Photochemical degradation of riboflavin, *J. Am. Chem. Soc.*, 1963, **85**, 3285-3287.

48 P. F. Heelis, The photophysical and photochemical properties of flavins (Isoalloxazines), *Chem. Soc. Rev.*, 1982, 11,15-39.

49 R. A. Larson, P. L. Stackhouse and T. O. Crowley, Riboflavin tetraacetate: A

View Article Online
DOI: 10.1039/C6RA23440B

potentially useful photosensitizing agent for the treatment of contaminated waters, *Environ. Sci. Technol.*, 1992, **26**, 1792-1798.

50 S. S. Kumar, T. P. A. Devasagayam, B. Bhushan and N. C. Verma, Scavenging of reactive oxygen species by chlorophyllin: an ESR study, *Free Radic. Res.*, 2001, **35**, 563-574.

51 P. Pieta, A. Petr, W. Kutner and L. Dunsch, In situ ESR spectroscopic evidence of the spin-trapped superoxide radical, $O_2^{\bullet-}$, electrochemically generated in DMSO at room temperature, *Electrochim. Acta.*, 2008, 53, 3412-3415.

52 J. L. Roberts, M. M. Morrison and D. T. Sawyer, Base-induced generation of superoxide ion and hydroxyl radical from hydrogen peroxide, *J. Am. Chem. Soc.*, 1978, **100**, 329-330.

53 M. J. Burkitt and R. P. Mason, Direct evidence for in vivo hydroxyl-radical generation in experimental iron overload: an ESR spin-trapping investigation, *Proc. Natl. Acad. Sci. USA.*, 1991, **88**, 8440-8444.

View Article Online
DOI: 10.1039/C6RA23440B

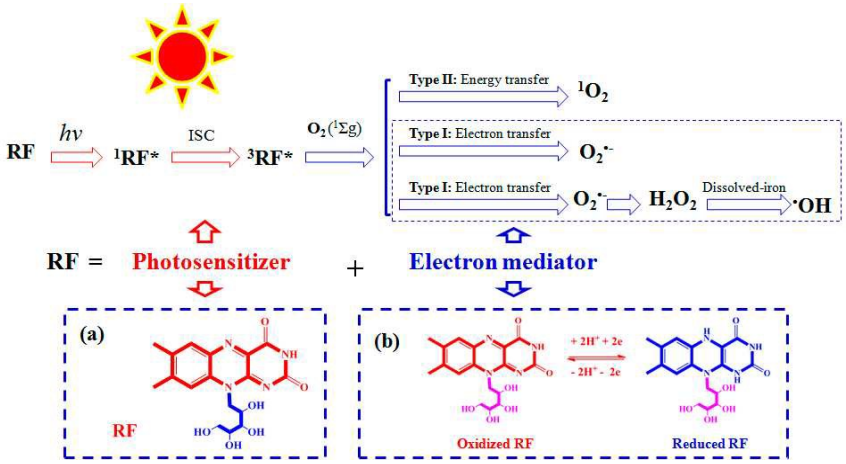

Fig. 1. Schematic illustration of RF-initiated ROS generation under visible irradiation (RF: Riboflavin; ISC: Intersystem Crossing).

View Article Online
DOI: 10.1039/C6RA23440B

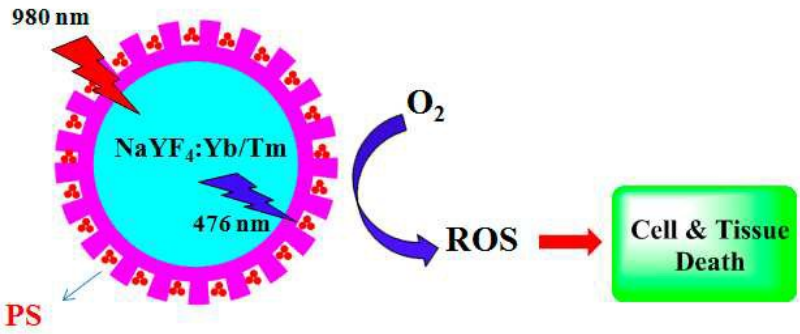

Fig. 2. Schematic illustration of the PS/UCNP nanoplatform for PDT and Proposed NIR-triggered ROS generation leading to oxidative damage of cancer cells, RTA (2',3',4',5'-tetraacetylriboflavin, a chemical derivative from RF) was used as PDT agent.

View Article Online
DOI: 10.1039/C6RA23440B

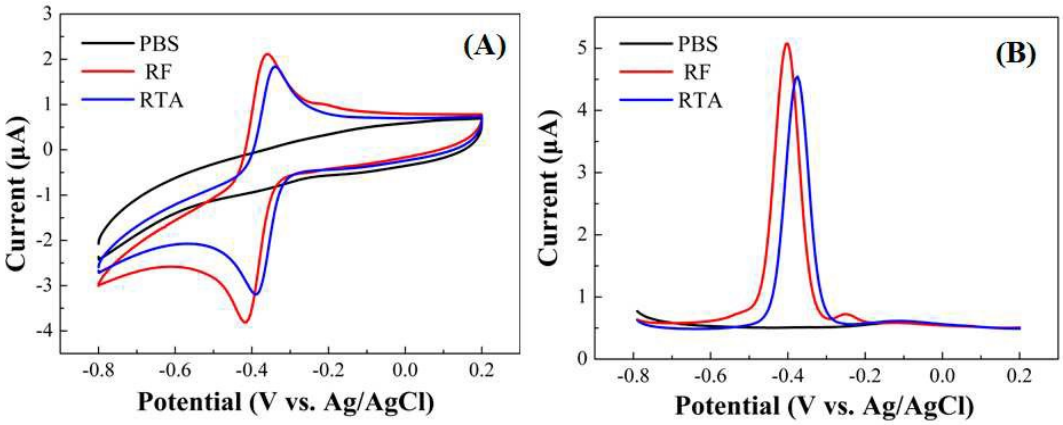

Fig. 3. (**A**) Cyclic voltammetry (CV) analysis of RTA (blue), RF (red) and 0.1 M PBS (pH 7.0, black) between -0.8 and 0.2 V vs. Ag/AgCl at a scan rate of 100 mV/s; (**B**) Differential pulse voltammetry (DPV) analysis RTA (blue), RF (red) and 0.1 M PBS (pH 7.0, black) between -0.8 and 0.2 V vs. Ag/AgCl at a scan rate of 100 mV/s.

View Article Online
DOI: 10.1039/C6RA23440B

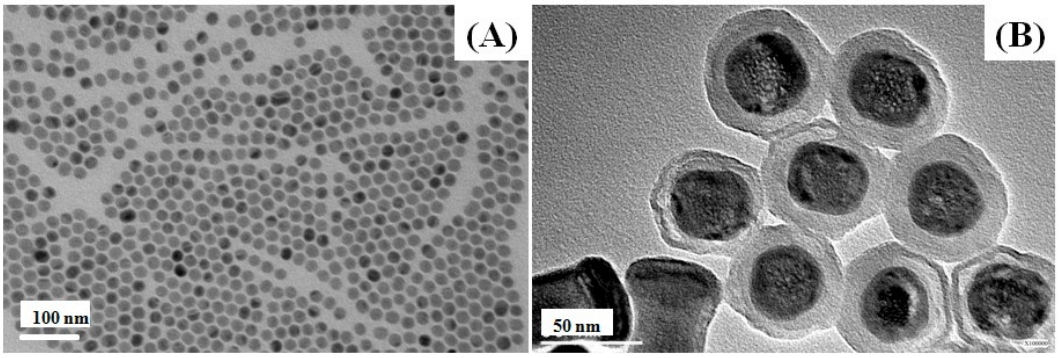

Fig. 4. (A) TEM image of $NaYF_4$:Yb/Tm nanoparticles; and **(B)** TEM image of mesoporous silica-coated $NaYF_4$:Yb/Tm nanoparticles.

View Article Online
DOI: 10.1039/C6RA23440B

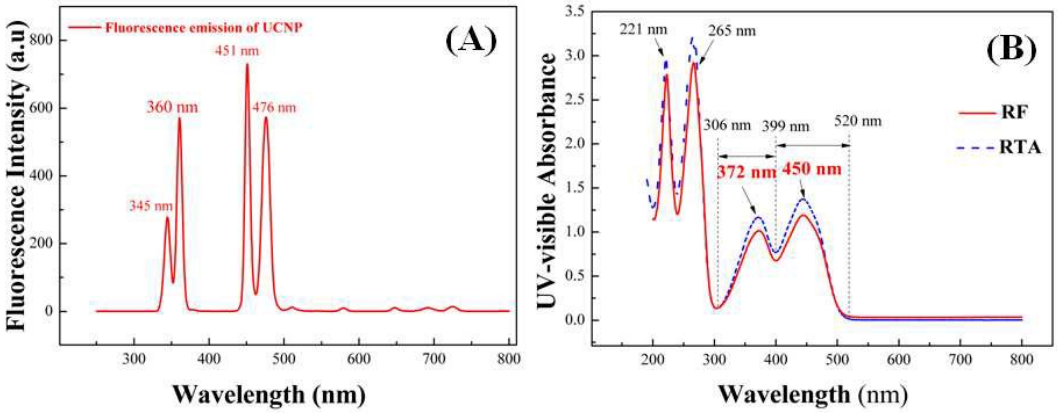

Fig. 5. (A) Emission fluorescence spectrum of $NaYF_4$:Yb/Tm nanoparticles excited under 980nm-NIR irradiation; and (**B**) UV-visible absorbance spectra of the RTA and RF solutions.

View Article Online
DOI: 10.1039/C6RA23440B

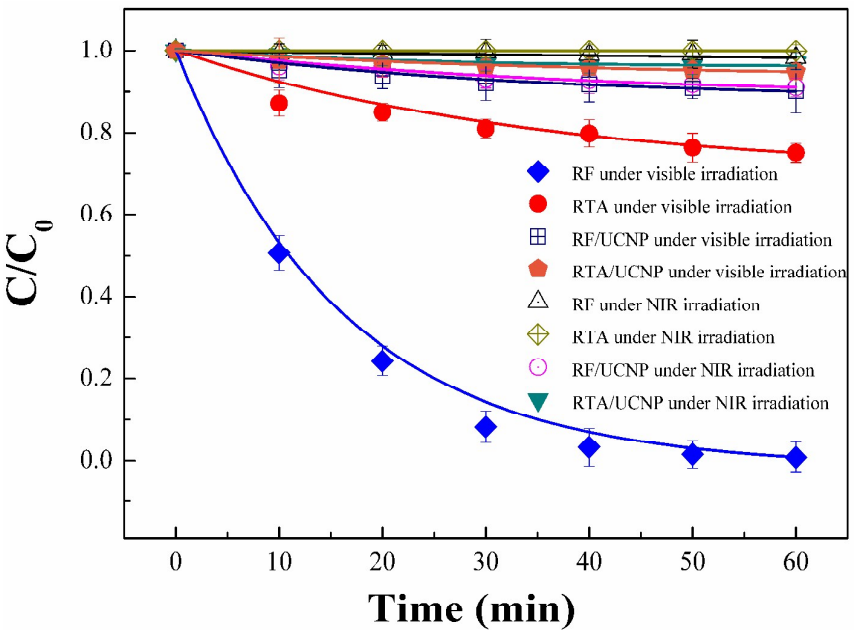

Fig. 6. Photostabilities of RF, RTA, RF/UCNP, and RTA/UCNP under diffierent conditions (visible irradiation or 980nm-NIR irradiation). A 50-W Xe-arc lamp (XD-300, Nanjing Yanan Co., China) equipped with an UV-cutoff (>400 nm) was used as visible light source and a 980 nm NIR laser (MDL-980, Changchun New industries optoelectronics tech. Co., China) was used as NIR light source. Initial concentrations of different solutions: RF solution of 10 μM; RTA solution of 10 μM; RF/UCNP solution of 5 mg/mL; RTA/UCNP solution of 5 mg/mL).

View Article Online
DOI: 10.1039/C6RA23440B

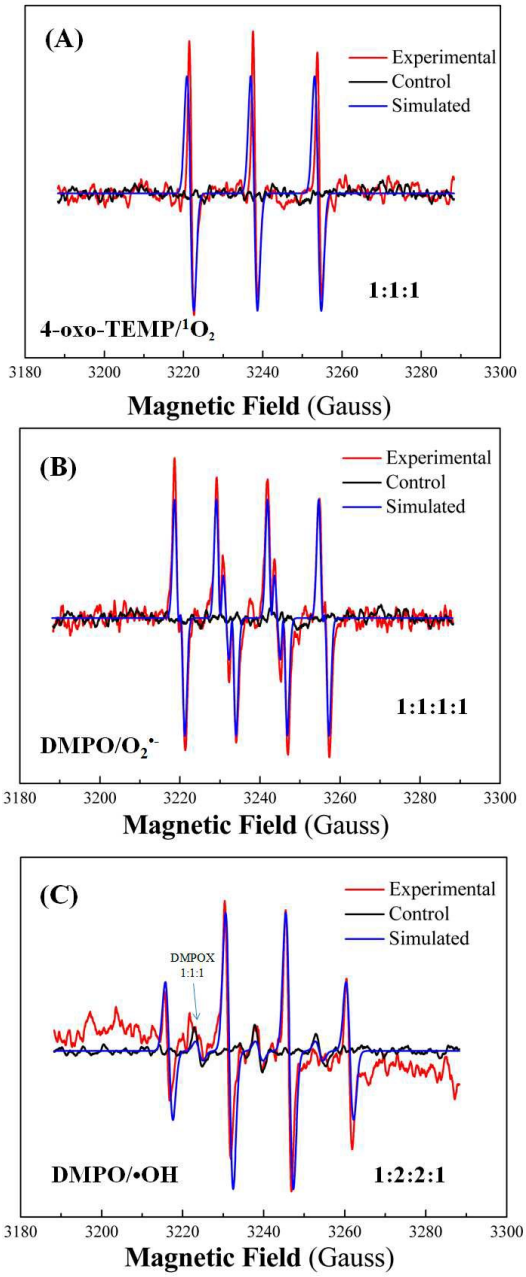

Fig. 7. ROS generation in RTA/UCNP solution (5 mg/mL) under NIR irradiation (980 nm): **(A)** EPR spectra of 4-oxo-TEMP/$^1O_2$ generated in aqueous solution (pH 7.0) and Simulation of EPR spectra of 4-oxo-TEMP/$^1O_2$; **(B)** EPR spectra of the DMPO/$O_2^{\bullet-}$ generated in VB_2 solution (dimethyl sulfoxide) and Simulation of EPR spectra of DMPO/$O_2^{\bullet-}$; and **(C)** EPR spectra of DMPO/•OH produced by RTA/UCNP solution (pH 3.0) in the presence of Fe^{2+} (5 μM) and Simulation of EPR spectra of DMPO/•OH.

View Article Online
DOI: 10.1039/C6RA23440B

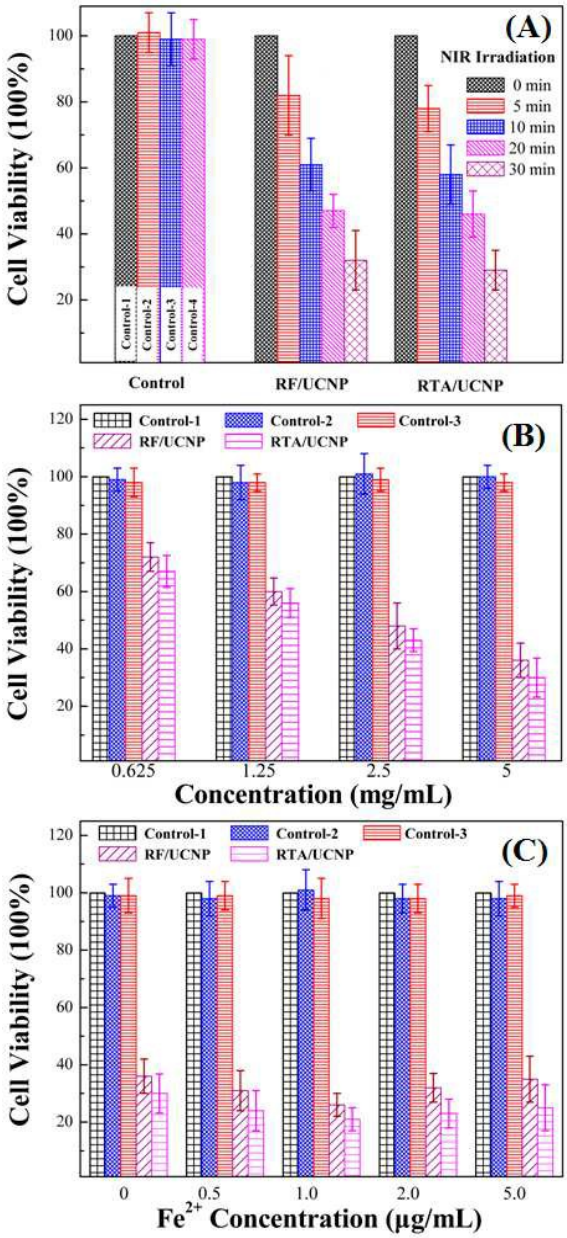

Fig. 8. MDA-MB-231 cancer cell viability: **(A)** PS/UCNP composites (5 mg/mL) after different exposure time to 980nm-NIR irradiation (5, 10, 20, and 30min); **(B)** Different concentration of PS/UCNP (0.625, 1.25, 2.5, and 5 mg/mL) after 10-minute NIR irradiation; and **(C)** Effect of Fe^{2+} under 980 nm-NIR irradiation. 48 hours after irradiation, cell death was measured and bar graphs represent means of triplicates±standard deviation.

View Article Online
DOI: 10.1039/C6RA23440B

Graphical Abstract